Bio-inspired hydrophobicity promotes CO2 reduction on a Cu surface

David Wakerley, Sarah Lamaison, Francois Ozanam, Nicolas F Menguy, Dimitri Mercier, Philippe Marcus, Marc Fontecave, Victor Mougel

Bio-inspired hydrophobicity promotes CO_2 reduction on a Cu surface

David Wakerley[a], Sarah Lamaison[a], François Ozanam[b], Nicolas Menguy[c], Dimitri Mercier[d], Philippe Marcus[d], Marc Fontecave[a]* and Victor Mougel[a]*

[a]*Laboratoire de Chimie des Processus Biologiques*, CNRS UMR 8229, Collège de France, 11 Place Marcelin Berthelot, Paris, France

[b]*Laboratoire de Physique de la Matière Condensée*, CNRS-École Polytechnique, Palaiseau Cédex, France

[c]*Sorbonne Université, UMR CNRS 7590, MNHN, IRD, Institut de Minéralogie, de Physique des Matériaux et de Cosmochimie, IMPMC,* 75005 Paris, France

[d]*Physical Chemistry of Surfaces Group*, ChimieParisTech-CNRS, Institut de Recherche de Chimie Paris, 75005 Paris, France

Abstract

Aqueous electrocatalytic reduction of CO_2 into alcohol and hydrocarbon fuels presents a sustainable route towards energy-rich chemical feedstocks. Cu is the only material able to catalyse the substantial formation of multi-carbon products (C_2/C_3), however competing proton reduction to hydrogen is an ever-present drain on selectivity. Herein, a superhydrophobic surface was generated by 1-octadecanethiol treatment of hierarchically structured Cu dendrites, inspired by the structure of gas-trapping cuticles on subaquatic spiders. The hydrophobic electrode attained 56% Faradaic efficiency for ethylene and 17% for ethanol production at neutral pH, compared to 9% and 4% on a hydrophilic, wettable equivalent. These observations are assigned to trapped gases at the hydrophobic Cu surface, which increase the concentration of CO_2 at the electrode|solution interface and consequently increase CO_2 reduction selectivity. Hydrophobicity is thus proposed as a governing factor in CO_2 reduction selectivity and can help explain trends seen on previously reported electrocatalysts.

Introduction

Figure 1a shows a theorized sustainable energy cycle propagated through the storage of renewable energies as CO_2-derived fuel. Such a process would provide relief to numerous environmental concerns, both current and impending,[1] and curtail dependency on fossil fuel. The cycle is driven through aqueous CO_2 electrolysis, wherein electrons and protons from water oxidation are used in the reduction of CO_2 to hydrocarbons and alcohols. Contemporary research now seeks an efficient and inexpensive catalyst for this reduction.

Cu remains the paradigmatic surface for CO_2 reduction, with the ability to produce C_2 and C_3 species, such as ethylene, ethanol and *n*-propanol.[2] Formation of such products has various thermodynamic and kinetic demands and requires multiple proton and electron transfers (Figure 1b). These are readily facilitated in water, however proton reduction to H_2 is more facile than CO_2 reduction (red dot, Figure 1b).[3] Water is also in substantial excess, due to the low solubility of CO_2 (33 mM at room temperature),[4] and as a result Cu electrodes will typically lose >30% Faradaic efficiency (FE) to H_2 production.[5]

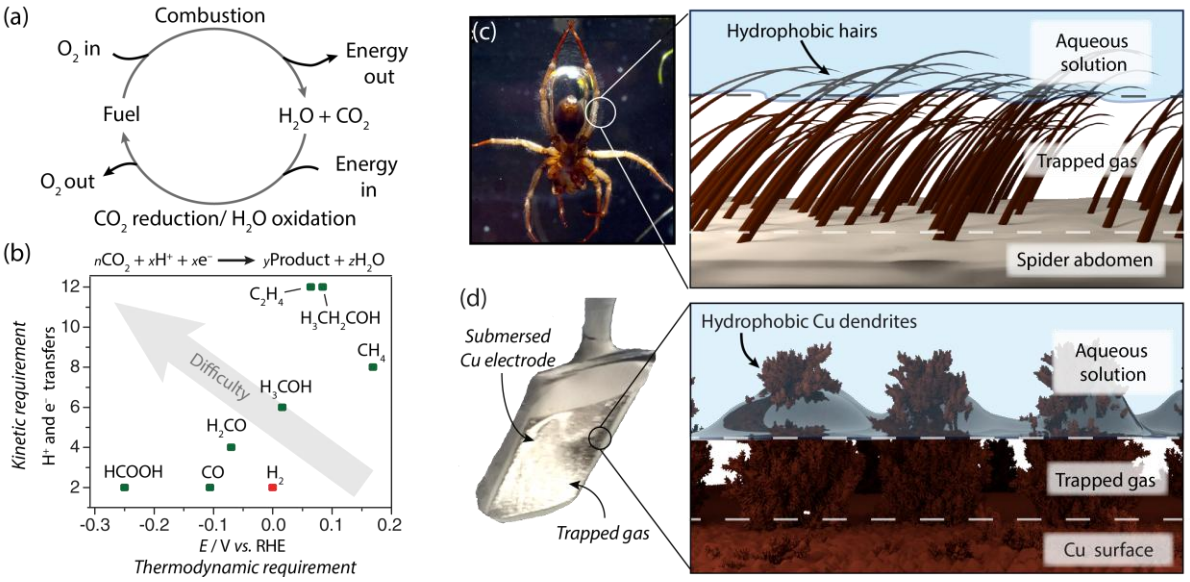

Figure 1 | CO_2 reduction as a source of sustainable fuel and an introduction to the 'plastron effect'. (a) The generation of renewable fuel through CO_2 reduction and H_2O oxidation. (b) The thermodynamic *vs.* kinetic requirement of various CO_2-reduction reactions.[3] The plotted values are based on the reaction equation given above the graph, made stoichiometric according to the product composition. (c, d) The 'plastron effect'; use of a hydrophobic surface to trap a layer of gas between the solution|solid interface. This is illustrated on a naturally occurring diving bell spider for subaquatic breathing in (c), and a hydrophobic dendritic Cu surface for aqueous CO_2 reduction in (d). Photo of the diving bell spider was adapted from reference 6 with permission by The Company of Biologists.

Improving selectivity towards CO_2 reduction, particularly towards products containing multiple carbons, remains a major priority in this field. Hitherto implemented strategies have included surface modifications,[7,8] adjusting surface pH[9] and the use of non-aqueous solvents,[10] however the most effective approaches can be summarised into three categories: *(1) Morphology*: nanowires,[11] nanowhiskers,[12] nanoparticles,[13] nanoprisms[14] and nanodendrites[15,16] present high catalytic surface areas that have shown appreciable selectivity. *(2) Carbon supports:* carbon frameworks and gas diffusion layers loaded with Cu have shown generation of C_2 products up to 80%.[17–20] *(3) Oxide*

layers: Surface oxides serve as precursors to active Cu catalysts, leading to efficiencies as high as 60% for ethylene formation.[21–23]

These strategies may also increase the hydrophobicity of an electrode, however this is rarely discussed as a determinant on selectivity.[2] Submerged hydrophobic surfaces trap appreciable amounts of gas at the nanoscale,[24,25] and even at the microscale if the Cassie-Baxter regime is reached,[26] allowing trapped CO_2 to accumulate at the Cu|solution interface. Recent reports have exploited gas|electrode|solution triple-phase boundaries to increase the CO_2 reduction activity of Cu on gas diffusion electrodes with hydrophobic polytetrafluoroethylene layers,[19,20] however it is difficult to assign this enhancement solely to hydrophobicity over other factors, such as their porosity and increased mass transport.[27] Herein, we thus study hydrophobicity as an isolated parameter on a Cu surface to establish its role in promoting gas-trapping and consequently selective CO_2 reduction.

Taking nature as inspiration, we introduce hydrophobicity based on the 'plastron effect' used by aquatic arachnids, such as the diving bell spider in Figure 1c.[28] These plastrons are composed of hydrophobic hairs that trap air, thereby allowing the spider to respire underwater. The gas-trapping phenomenon occurs when hydrophobic surface chemistry is presented on the microscale and nanoscale simultaneously.[29] We achieve an analogous multi-scale hydrophobic surface through modification of hierarchically structured dendritic Cu with a monolayer of waxy alkanethiol. The resultant electrode visibly traps CO_2 gas at the electrolyte|electrode interface, forming a triple-phase boundary (Figure 1d). As a result, H_2 evolution was substantially lowered in CO_2-saturated electrolyte compared to an unmodified hydrophilic equivalent, from 71% FE to 10%, while CO_2 reduction increased from 24% to 86%, of which C_2 products comprised 74%. The drastically increased CO_2 concentration at the hydrophobic Cu surface was identified as key to the increased catalytic selectivity, which we propose is present in other reported systems.

Preparation and characterization of the hydrophobic Cu dendrite

Cu dendrite scaffolds were grown using previously reported aqueous electrodeposition procedures, forming hierarchical architectures with both micro and nanoscale features (Supplementary Figure 1).[30,31] Powder X-ray diffraction (PXRD) measurements confirmed the structure to be metallic Cu (Figure 2a), although a small amount of Cu_2O was visible (Supplementary Figure 2). The hydrophobic treatment was undertaken by submersing the dendritic Cu into liquid 1-octadecanethiol at 60°C for 15 minutes to form an alkanethiol layer. Transmission electron microscopy (TEM) of the dendritic Cu after treatment confirmed the nanostructure remained intact (Figure 2b) and was coated with a monolayer between 2-3 nm in thickness (Figure 2c), consistent with a surface of 1-octadecanethiol molecules bound upright (chain length is 2.3 nm between surface-bound S and terminal C). The carbonaceous nature of the coating was confirmed by energy-filtered transmission electron microscopy (EF-TEM) at the C-K edge (Figure 2d). X-ray energy-dispersive spectroscopy (XEDS) of the area indicated in Figure 2d displayed S and C environments within the layer (Supplementary Figure 3) and no carbonaceous layer was present on untreated Cu dendrite (Supplementary Figure 4).

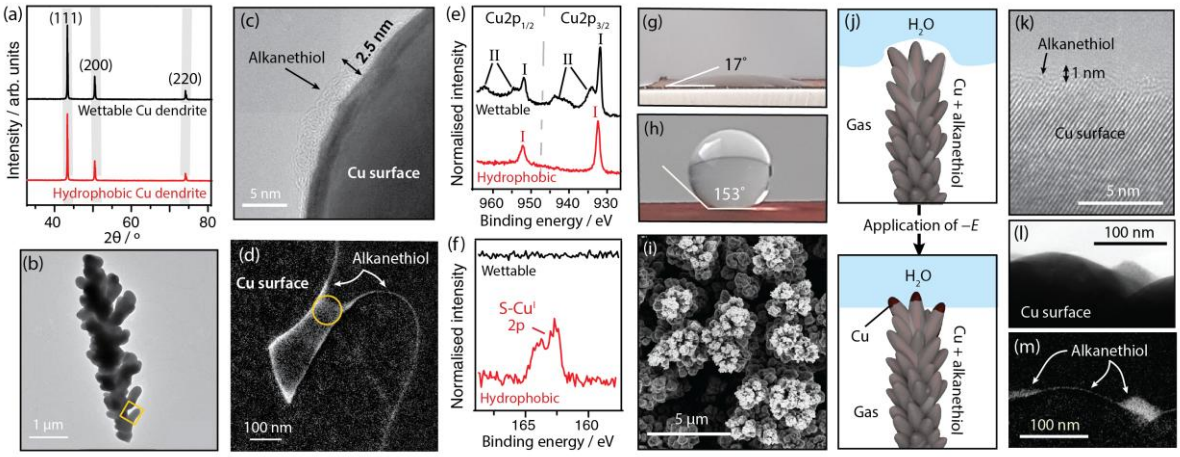

Figure 2 | Characterization of the electrode surface. (a) PXRD of Cu dendrite with and without hydrophobic surface treatment. (b,c) TEM and high-resolution TEM images of a 1-octadecanethiol-treated Cu dendrite showing the layer of alkanethiol attached to the Cu surface, the yellow square in (b) indicates the area observed in (d). (d) EF-TEM using the C-K edge of an alkanethiol-treated Cu dendrite surface, the yellow circle indicates the area used for TEM-XEDS analysis in Supplementary Figure 3. (e) XPS spectra in the Cu regions showing peaks assigned to I and II oxidation states. (f) XPS spectra showing the presence of S on the alkanethiol-treated Cu surface. (g) and (h) show contact angle measurements of the *wettable* and *hydrophobic dendrite* respectively. (i) SEM image of the *hydrophobic dendrite* after 2.5 hours of applied cathodic potential in 0.1 M $CsHCO_3$ (CO_2 saturated, pH 6.8, room temperature) with a CO_2 flow of 10 ml min^{-1}. (j) Illustration of the *hydrophobic dendrite* gaining a solid|liquid interface upon application of negative potential. (k), (l) and (m) show the equivalent images from (c) and (d) after electrolysis in 0.1 M $CsHCO_3$ (CO_2 saturated, pH 6.8, room temperature) with a CO_2 flow of 10 ml min^{-1} for 30 minutes at –1.4 V vs. RHE.

The alkanethiolation removes Cu oxide from the surface, leaving Cu–S bonds, as illustrated by X-ray photoelectron spectroscopy (XPS, Figure 2e).[32] Before treatment, the Cu dendrite shows environments consistent with Cu^{I}_2O at 932.5/952.4 eV and $Cu^{II}O$ at 934.6/955.0 eV and 942.8/962.7 eV. Analysis of the Cu LMM Auger showed no evidence of metallic Cu^0 at the surface (Supplementary Figure 5).[33] After reaction with 1-octadecanethiol all Cu^{II} environments are removed, forming a

surface of Cu^{I} (Figure 2e and Supplementary Table 1), and a new S 2p peak is visible at 163.0 eV, consistent with Cu–S bonds (Figure 2f).[33] The presence of the alkanethiol layer was further confirmed through attenuated total reflectance infrared (ATR-IR) spectroscopy (Supplementary Figure 6).

Contact angle measurements illustrated that without 1-octadecanethiol modification the Cu dendrite surface is hydrophilic; a deposited water droplet sat with a contact angle of 17° (Figure 2g). The alkanethiol-treated electrode is not susceptible to the same wetting, with a drastically increased contact angle of 153° (Figure 2h), falling into the regime of superhydrophobicity where trapped gases are expected on both the micro and nanoscale.[34] For clarity, these electrodes will be referred to as the *wettable dendrite* and *hydrophobic dendrite* for the hydrophilic and hydrophobic dendritic Cu surfaces, respectively.

Initial characterization of the dendrites' electrochemical properties revealed a significant decrease in electrochemically-active surface area (ECSA) upon introduction of hydrophobicity. Capacitance measurements of the *hydrophobic dendrite* indicated the surface had very limited electrical contact with the solution, displaying an ECSA of 3×10^{-3} cm^2 cm^{-2}, much lower than the 21 cm^2 cm^{-2} obtained on the *wettable dendrite* (where cm^2 cm^{-2} indicates the ECSA of the dendritic electrode *vs*. that of a flat electrode, Supplementary Figure 7). BET analysis through Kr adsorption measurements revealed that the ECSA disparity is not from a loss in geometric surface area upon alkanethiol treatment, as these remained similar: 90 cm^2 cm^{-2} and 92 cm^2 cm^{-2} for the *wettable dendrite* and *hydrophobic dendrite*, respectively (where cm^2 cm^{-2} indicates the BET-derived surface area of the dendritic electrode *vs*. the area of a flat electrode). The decrease in ECSA is therefore induced by gas trapping at the interface between the *hydrophobic dendrite* and solution, as illustrated in Figure 2j (top panel).

Upon application of reducing potential over 60 minutes in aqueous electrolyte (0.1 M $CsHCO_3$, CO_2 saturated) the ECSA of the *hydrophobic dendrite* electrode increased to 0.2 cm^2 cm^{-2} (Supplementary

Figure 7b), which can also be seen through linear sweep voltammetry (LSV, Supplementary Figure 8). This increase is assigned to loss of 1% of alkanethiol when reaching labile Cu^0 oxidation states, as the ECSA is 1% of the *wettable dendrite* (21 $cm^2\ cm^{-2}$). This loss occurs at the point of the electrode closest to the electrolyte, as suggested through SEM images that show brighter Cu regions at the tips of the dendrite (Figure 2i and Supplementary Figure 9). Similar activation has been documented on other hydrophobic electrodes.[26] The *hydrophobic dendrite* therefore requires an initial application of potential to generate a stable liquid|electrode|gas triple-phase boundary at the top of the dendrite where electrochemical reactions take place, as illustrated in Figure 2j. This activation was monitored through one day of repeated LSV scans, wherein the current at –1.4 V *vs.* RHE stabilised 3-5 times lower than that of the *wettable* equivalent (Supplementary Figure 10).

To ensure the *hydrophobic dendrite* maintained its hydrophobicity upon application of potential, contact angle measurements were carried out after 12 hours of electrolysis at –15 mA cm^{-2} (Supplementary Figure 11). The resultant angle of 143° indicated that the hydrophobic surface treatment was not removed. Furthermore, ^{1}H-NMR spectroscopy showed no 1-octadecanethiol within the electrolyte after electrolysis (Supplementary Figure 12), although some dissolved alkanethiol may be present below the detection limit of the experiment. XPS analysis before and after electrolysis showed similar ratios of Cu:S on the sample (Supplementary Table 2), however a portion of the 1-octadecanethiol is converted into alkanesulfonates (Supplementary Figure 5c, 168.6 eV), which is known to occur upon exposure of alkanethiol monolayers to air.[35] Nevertheless, HR-TEM and EF-TEM at the C-K edge (Figure 2k, l and m) do show the monolayer loses density and that large carbonaceous deposits are present on the nanostructure after electrolysis. We thus propose that the majority of the C_{18}-alkane chain does not dissolve from the electrode surface, but a portion may move across the surface to form aliphatic agglomerates, explaining how the surface maintains hydrophobicity whilst allowing current to pass.

Comparing the catalytic activity of *hydrophobic* and *wettable* Cu dendrites

Figure 3a shows the LSV of the *hydrophobic dendrite* and equivalent *wettable dendrite* in CO_2–saturated $CsHCO_3$ electrolyte (0.1 M, pH 6.8). Cs^+ cations were used due to their superior ability to buffer pH changes at the electrode|solution interface during electrolysis compared to other cations,[36] thereby eliminating changes in surface pH as a determinant on selectivity. To reach a current of –5 mA cm^{-2}, the *wettable dendrite* required a potential of –0.68 V *vs.* RHE, while the *hydrophobic dendrite* required a more negative potential of –1.38 V *vs.* RHE. The lowered current at a given potential can be partly explained by the significantly lower ECSA of the *hydrophobic dendrite* but should also be assigned to the lack of proton reduction activity exhibited by this electrode. Controlled potential electrolysis (CPE) confirmed this, as even at highly cathodic potentials the *hydrophobic dendrite* has vastly lowered H_2 evolution activity: At –1.6 V *vs.* RHE, the *hydrophobic dendrite* displays H_2 evolution activity below 10%, while the *wettable* displays values above 60% (Figure 3b and 3c). In place of H_2 evolution, the *hydrophobic dendrite* presents superior CO_2 reduction efficiency for both C_1 and C_2 products (Figures 3b and c), except at –1.2 V *vs.* RHE, at which point current was too low for detection of C_2 products (Supplementary Figure 13). To confirm that the optimal CO_2 reduction selectivity on the *wettable dendrite* was not attained at lower potentials, CPE at less cathodic biases was carried out (Supplementary Figure 14).

During electrolysis, CO_2 was introduced as a stream of gas from the bottom of the cell (illustration provided in Supplementary Figure 15). When using the *hydrophobic dendrite,* the capture and retention of the gaseous CO_2 stream was observed, causing a bubble to engulf the entire electrode surface (Figure 3e, Supplementary Video 1). If the gas flow was not incident to the *hydrophobic dendrite* to constantly refill this bubble, formation of C_1 and C_2 products was severely reduced (Figure 3d), indicating that the captured CO_2 at the electrode surface is the predominant substrate of the *hydrophobic dendrite*. At lower partial pressures of CO_2 in the gas stream, the CO_2 reduction rate dropped accordingly (Supplementary Figure 16).

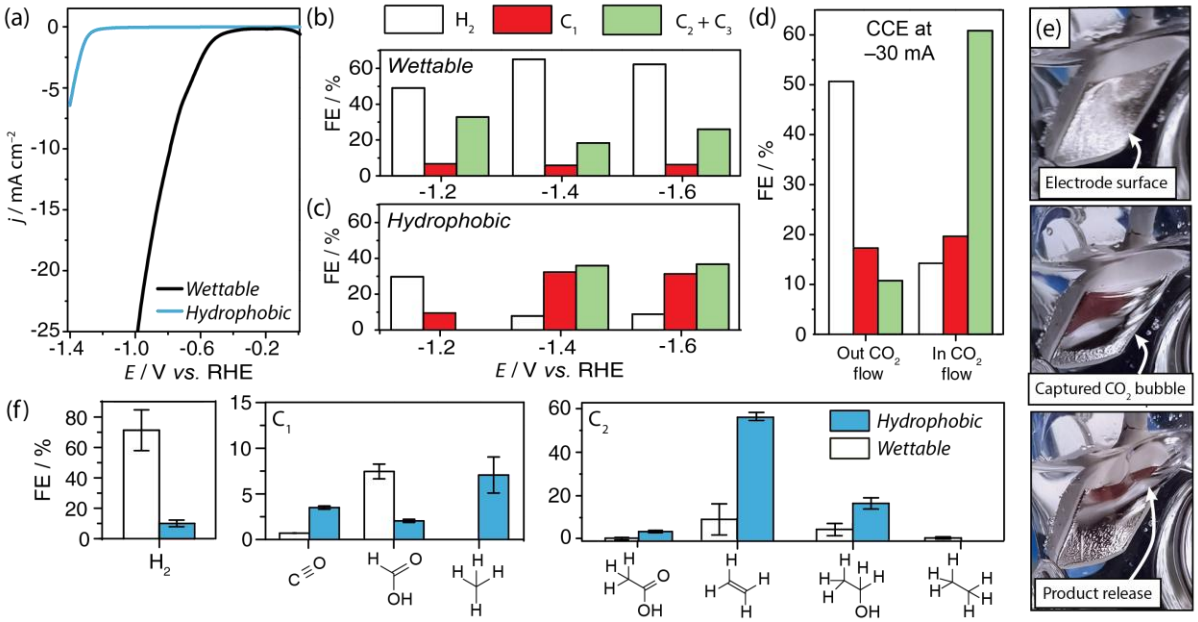

Figure 3 | The effect of hydrophobicity on electrocatalytic CO_2 reduction. (a) Linear sweep voltammogram of the *wettable* and *hydrophobic dendrite* (v = 20 mV s^{-1}). (b,c) Controlled potential electrolysis product FEs from the *wettable* and *hydrophobic* dendrite at various potentials. (d) Product formation FE at the *hydrophobic dendrite* after controlled current electrolysis at –30 mA cm^{-2} inside of and outside of the CO_2 flow at 2.5 ml min^{-1}. (e) Photos of the capture and release of a CO_2 bubble on the *hydrophobic dendrite* surface. (f) Product formation FEs at the *hydrophobic vs. wettable dendrite* when passing an overall current density of –30 mA cm^{-2}. In all cases the electrolyte was CO_2-saturated $CsHCO_3$ (0.1 M, pH 6.8, room temperature). Unless stated otherwise, a CO_2 flow rate of 5 ml min^{-1} was used throughout electrolysis. Gaseous products were analysed after 10 and 30 minutes and liquid products after 35 minutes of electrolysis. Error bars are based on the standard deviation of 3 individual measurements.

Control experiments without hierarchical Cu surface morphology were undertaken using a flat Cu electrode treated with 1-octadecanethiol. Neither gas trapping nor large contact angles were observed (contact angle: 90°, Supplementary Figure 17) and the electrode did not show a drastic increase in selectivity for CO_2 reduction compared to a pristine Cu electrode (see Supplementary

Table 3). The combination of hydrophobic treatment and hierarchical morphology therefore facilitate gas trapping.

Controlled current electrolysis (CCE) at –30 mA cm^{-2} for the two Cu dendrites was undertaken to understand their selectivity while exerting the same mass transport pressure on the solution (Figure 3f). The *hydrophobic dendrite* required a higher cathodic applied potential to reach –30 mA cm^{-2} (E = –1.1 V-–1.5 V *vs.* RHE, IR corrected), but had much higher selectivity for CO_2 reduction: CO (3% *hydrophobic;* 1% *wettable*), methane (7% *hydrophobic;* 0% *wettable*), ethylene (56% *hydrophobic;* 9% *wettable*) ethanol (17% *hydrophobic;* 4% *wettable*) and acetic acid (1% *hydrophobic;* 0.4% *wettable*). In contrast, the *wettable dendrite* required a less cathodic potential to reach –30 mA cm^{-2} (E = –0.8 V-–1.0 V *vs.* RHE, IR corrected) as it carried out mostly H_2 evolution (10% *hydrophobic;* 71% *wettable*), however it also showed the highest selectivity for formate (2% *hydrophobic;* 7% *wettable*), ethane (0 % *hydrophobic;* 0.5% *wettable*) and *n*-propanol formation (0 % *hydrophobic;* 2% *wettable, not pictured*). The *hydrophobic dendrite's* selectivity for C_2 products (74% total) rivals that of state-of-the-art gas-diffusion electrode systems in alkaline conditions (66% ethylene, 11% ethanol, 6% acetate),[20] however the achieved currents and overpotentials are poorer in the neutral pH electrolyte.

Extended CO_2 reduction on the *hydrophobic dendrite* over 5 hours at a controlled current density of –30 mA cm^{-2} showed a high ethylene and ethanol efficiency of 30%-55% and 12-22%, respectively (Supplementary Figure 18). During the experiment, C_2 product formation was again sensitive to interaction with inbound CO_2: drops in C_2 production were observed when CO_2 flow fell out of line with the electrode surface (Supplementary Figure 18, as indicated), however the stream could be adjusted to restore activity. Despite this, a gradual decrease in C_2 production activity was apparent, coinciding with destruction of regions of the dendrite surface (Supplementary Figure 19). This destruction is assigned to the mechanical stress imposed by continual collision of bubbles with the electrode surface. Engineering-efforts using vapor-fed electrodes to relieve this stress are ongoing.

The gas-trapping of the *hydrophobic dendrite* could also be exploited for CO reduction, where low substrate concentration is particularly problematic ([CO] = 1 mM at 1 atm at room temperature).[4] CCE at –30 mA cm^{-2} in a CO flow on the *hydrophobic dendrite* showed 23.5% FE for CO reduction, compared to 0.88% on the *wettable dendrite* in 1 M KOH (Supplementary Figure 20, Supplementary Table 4). Further experiments showed that C_2 selectivity during CO reduction on the *hydrophobic dendrite* is greatly promoted in pH 14 solution (1 M KOH C_1: C_2 ratio = 1:24), in comparison to pH 7 (0.1 M KPi C_1:C_2 ratio = 1:1.7, Supplementary Figure 20). Additional CO_2 reduction experiments in more acidic conditions (pH 4.6, CO_2-saturated 0.1 M KPi) similarly showed a decrease in C_2 selectivity (C_1:C_2 ratio = 1:0.8, Supplementary Figure 21, Supplementary Table 5). Formic acid reduction experiments produced only H_2, excluding it as a source of C_2 products (Supplementary Table 6).

Explanation of the reported data is given in Figure 4a-d, which show a single strand of the dendritic Cu in its *wettable* (Figure 4a and b) and *hydrophobic* form (Figure 4c and d). Since highly cathodic potentials are applied, it is assumed that both the dendrites react rapidly with either H^+ or CO_2 to form Cu–H* or Cu–COOH* intermediates respectively,[37] and therefore selectivity is controlled by mass transport of the two substrates. The *wettable dendrite* has a large liquid|electrode interface therefore only dissolved H^+/CO_2 are substrates (Figure 4a). A higher proportion of Cu–H* groups is then expected, which promotes H_2 formation (Figure 4b). On the other hand, the electrolyte is pushed away from the *hydrophobic dendrite* Cu surface, forming an electrolyte|solid|gas triple-phase boundary at the electrode (Figure 4c). CO_2 mass transport is then omnidirectional, while H^+ comes unilaterally from bulk solution, which drastically increases the local CO_2 concentration. The surface concentration of Cu–COOH* and the subsequently formed Cu–CO* is then greatly increased over Cu–H*. This promotes C–C coupling and therefore the efficiency for C_2 products is increased (Figure 4d). Reduction of CO without coupling is also possible, explaining the enhanced CH_4 production. Based on the presented CO reduction experiments, the selectivity for C_2 over CH_4 can be increased with high solution pH, corroborating recent reports that C_2 formation at high overpotential

is dependent on high concentrations of Cu–CO*, while CH_4 formation requires a rate-limiting electron-proton transfer to a Cu–CHOH* intermediate.[38]

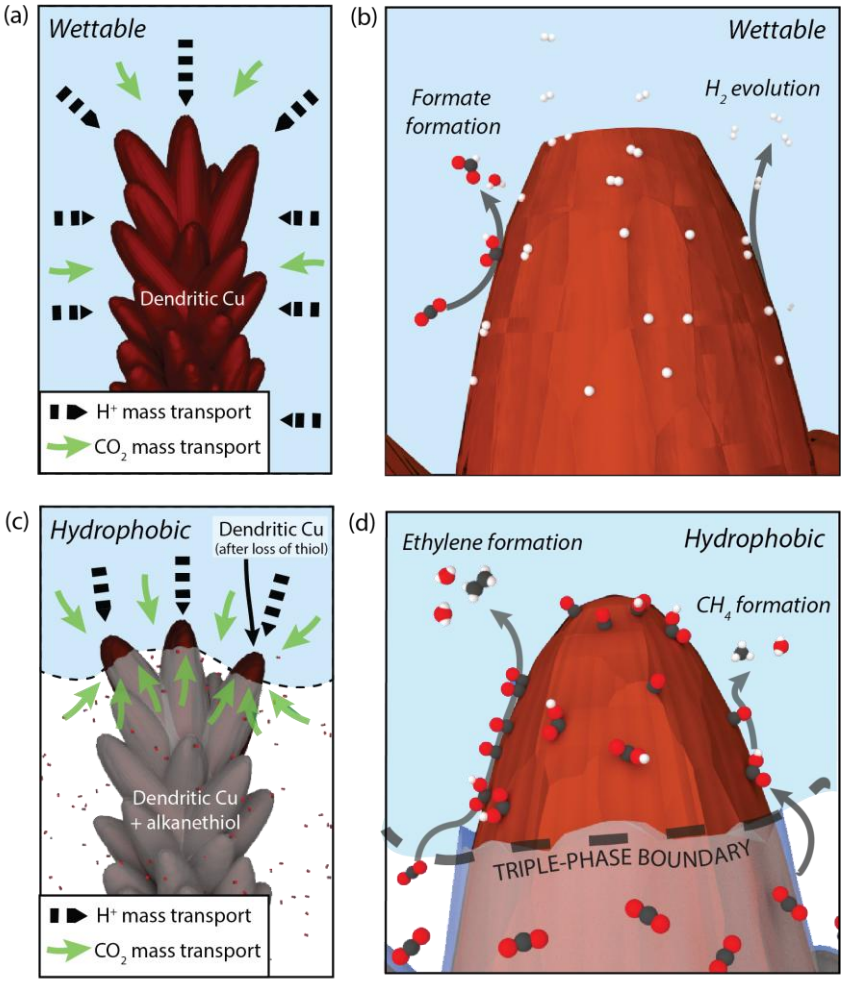

Figure 4 | The proposed role of hydrophobicity in promoting CO_2 reduction over proton reduction. (a,b) The *wettable dendrite* under operation, showing reactant mass transport and product formation on the electrode surface. (c, d) The operation of the *hydrophobic dendrite*, illustrating the enhanced CO_2 mass transport from the triple-phase boundary between electrolyte, electrode and gaseous CO_2 and the resultant formation of key products on the surface.

Perhaps more interesting are the products from CO_2 reduction produced solely on the *wettable dendrite*: ethane and *n*-propanol, albeit in small quantities (below 5%). The lack of these products on the *hydrophobic dendrite*, as well as other highly efficient C_2-forming electrodes,[20] suggests that

hydrogen transfer is a rate limiting step in their formation and therefore they require a high concentration of Cu–H*. This is supported by recent reports that show high efficiencies for CO_2 reduction to *n*-propanol with relatively high H_2-evolution activity[39] and also reports of ethane formation on surfaces that generate large quantities of H_2.[40]

The presented experiments led us to consider other reported catalysts for C_2 product formation, which have been traditionally Cu oxides.[23] Many explanations for their activity are available, but we hypothesize that the combination of nanostructured surfaces with hydrophobic Cu_2O[41] creates similar gaseous voids that trap CO_2 to create an electrolyte|electrode|gas triple-phase boundary. Regions not in contact with electrolyte solution on these surfaces would explain why oxides are still spectroscopically visible *in operando*,[12] despite their expected removal at cathodic potential.[42] It may also explain the low long-term stability of such surfaces, as removal of the oxides increases surface wettability. Further support for this concept is illustrated by stable C_2 production on gas-diffusion electrodes,[20] whose hydrophobicity is not as susceptible to reduction and as such maintain their electrolyte|electrode|gas interfaces.

Conclusion

In summary, a hydrophobic coating of long-chain alkanethiols on dendritic Cu, with no further modification, leads to a drastic increase in CO_2 reduction selectivity. The difference is a result of a plastron effect; a gaseous layer trapped at the surface of the electrode that increases the local CO_2 concentration, allowing the Cu dendrite to match the high selectivity for C_2 products reported on Cu-loaded gas-diffusion electrodes.[20] In the present form, the electrode suffers from some drawbacks for implementation in technological devices and future work will focus on promoting stable hydrophobicity on high-surface-area microporous electrodes to further increase activity.

We conclude that hydrophobicity, and the resultant gaseous voids that it introduces, is thus a governing factor of CO_2 reduction selectivity on Cu and should be considered in the future design and understanding of electrocatalytic surfaces for both CO_2 and CO reduction.

Methods

General: SEM images were performed on a SU-70 Hitachi FEGSEM fitted with an X-Max 50 mm^2 Oxford EDX spectrometer. PXRD was performed in Bragg-Brentano geometry using a BRUKER D8 Advance diffractometer with Cu Kα radiation ($\lambda K\alpha_1$=1.54056 Å, $\lambda K\alpha_2$=1.54439 Å) and a Lynxeye XE detector. Contact angle measurements were made on a slow-motion video camera with 15 µl of H_2O. XPS spectra were performed using a Thermo ESCALAB 250 X-ray photoelectron spectrometer with a monochromatic Al-Kα X-ray source ($h\nu$ = 1486.6 eV).

Preparation of Cu dendrites: Square Cu surfaces of 1 cm^2 surface area were prepared from a Cu plate (GoodFellow, 99.999%, 1 mm thickness) that had its sides, back and backside electrical contact encased in epoxy resin (Loctite, Henkel). The surface was polished mechanically using alumina micropolish on a polishing cloth (3 µm, Struers) followed by copious rinsing in water. Dendrite deposition was subsequently undertaken by applying –0.5 A cm^{-2} to the electrode for 120 s in a solution containing 0.1 M $CuSO_4 \cdot 5H_2O$ (99.9%, Sigma Aldrich) in 1.5 M H_2SO_4 (Sigma Aldrich) followed by rinsing under a gentle stream of water, then acetone. The electrode was then dried under a stream of air.

Alkanethiol deposition: Application of 1-octadecanethiol (Sigma, 98%) was undertaken by first melting the waxy solid under vacuum at 60 °C. The electrode to be treated was then submerged into the liquid under Ar and left for 15 minutes at 60 °C. After this point the electrode was moved to a solution of ethyl acetate at 60 °C to remove excess 1-octadecanethiol and allowed to dry in ambient conditions.

Electrocatalytic analysis: Electrochemical analysis was carried out in an air-tight two compartment electrochemical cell separated by a Nafion membrane (Alfa Aesar, N115) or bipolar membrane (Fuel cell store, Fumasep FBM). The counter electrode was a Pt wire (GoodFellow) and the reference a Ag/AgCl wire in KCl (3 M KCl, palmsens). The electrolyte was deaerated/saturated with CO_2/CO/Ar before each experiment by bubbling CO_2 (≥ 99.998%, Linde), CO (Linde) or Ar (Linde) for at least 10 minutes.

During electrolysis the electrodes were placed at a 45° incidence to the CO_2 inlet, as this ensured all bubbles of CO_2 from the bottom of the vessel would collide with the electrode surface. CO_2 was flowed through the cathode compartment of the cell using a mass flow controller (Brooks Instruments) and the solution was stirred. The headspace was connected to a gas chromatograph (GC, discussed below) and was typically sampled at 10 and 30 minutes. The liquid phase was analysed for products by ^{1}H-NMR after 35 minutes (see below). Faradaic efficiency was calculated based on the time before injection that was required to fill the GC injector sample loops (1 mL). This is summarised in Equation 1.

$$Faradaic\ efficiency\ (\%) = \frac{n_{product} \times n_{electrons} \times F}{(Q_{t=0} - Q_{t=x})} \times 100 \qquad \text{Equation 1}$$

Where $n_{product}$ is the product measured (mol), $n_{electrons}$ is the number of electrons to make said product from CO_2/H_2O or CO/H_2O, F is the Faraday constant (C mol^{-1}), $Q_{t=0}$ is the charge passed at the point of injection (C) and $Q_{t=x}$ is the charge passed at x seconds before injection, (x being the time required to fill the GC sample loop based on sample loop size and gas flow rate, C).

During LSVs the electrode was placed outside of the CO_2 inlet, no stirring was applied and CO_2 flow was decreased to 0.2 ml min^{-1}.

Potentials were converted to the Reversible Hydrogen Electrode (RHE) using the relationship: E (RHE) = E (Ag/AgCl) + 0.197 + (pH × 0.059). IR-drop correction of the potentials applied during controlled current electrolysis was undertaken manually using the resistance measured immediately after electrolysis was completed. The reported potentials are those measured at the time point of GC analysis (typically 10 or 30 minutes). IR-drop correction was not applied during controlled potential electrolysis, LSVs or CVs.

Electrochemically active surface area measurements: Electrochemically active surface area was measured through the capacitance of the electrodes in a 0.1 M solution of $CsHCO_3$ (Sigma, 99.9%) saturated with CO_2. Capacitance was measured by analysis of the electrode cyclic voltammogram at –0.15 V *vs.* the standard hydrogen electrode (SHE) using Equation 2:

$$\frac{ia-ic}{2} = Cv \qquad \text{Equation 2}$$

Where C is the capacitance (F), i_a is the anodic current at –0.15 V *vs.* SHE (A), i_c is the equivalent cathodic current (A) and v is the scan rate (V s^{-1}). The capacitance was found by plotting the left side of Equation 2 against scan rate. Electrochemically-active surface area was then determined from the difference between the capacitance of the nanostructured surfaces relative to a flat 1 cm^2 Cu surface.

Gas chromatography: Gas chromatography was carried out on an SRI instruments MG#5 GC with Ar carrier gas. H_2 was quantified using a thermal conductivity detector and separated from other gases with a HaySepD precolumn attached to a 3 m molecular sieve column. All carbon-based products were detected using a flame-ionisation detector equipped with a methanizer and were separated either using a 3 m molecular sieve column (CO, CH_4) or a 5 m HaySepD column (C_2H_4, C_2H_6). Calibration was performed using a custom mixture of each gas in CO_2.

^{1}H-NMR: ^{1}H-NMR spectroscopy was undertaken on a Bruker Avance III 300 MHz spectrometer at 300 K. A sample of the liquid phase electrolyte was taken and D_2O was added as a locking solvent, along with an aqueous terephthalic acid solution that served as a reference for quantification. A Pre-SAT180 water suppression method was carried out to remove the water peak from each spectrum.[43]

BET: Surface areas were obtained from analysis of Kr adsorption isotherms measured on a BelSorp Max set-up at 77 K. Prior to the measurement, samples were treated under vacuum at 130°C for at least 7 h. Surface areas were estimated using the BET model (Kr cross-sectional area 0.210 nm^2). The BET sample was prepared by undertaking the described dendrite preparation procedure on a large Cu surface (3x3 cm^2) to grow enough dendrite for measurement. Alkanethiol treatment of the large electrode was carried out by covering the dendrite in a powder of 1-octadecanethiol and inserting the resultant surface horizontally in a vacuum oven at 100^{o}C for 15 minutes. The electrode was subsequently removed and left in a bath of warm ethyl acetate at 60 ^{o}C for 5 minutes. Once dry, the dendritic Cu was carefully scraped off the underlying Cu support for analysis. The value derived from the BET measurement, reported in $m^2\ g^{-1}$, was converted to $cm^2\ cm^{-2}$ by multiplying it by the mass of deposited dendrite onto the 1 cm^2 flat Cu support (5 mg for the *wettable dendrite* and 4 mg for the *hydrophobic dendrite*).

TEM/STEM: Transmission electron microscopy images and chemical maps were acquired with a Jeol 2100F microscope operated at 200 kV and equipped with a UHR pole piece. XEDS spectra were acquired in STEM mode with the same microscope, equipped with a Jeol system for X-ray detection and cartography. Energy-Filtered TEM images at zero loss and C-K edge were acquired using a Gatan GIF 2991 spectrometer. Samples for TEM were prepared by shaking a lacey carbon TEM grid in a vial containing a small amount of Cu dendrite powder.

ATR-FTIR: Attenuated total reflectance-Fourier transform infrared spectroscopy was carried on a 0.5 mm thick Si-prism coated with 3-5 nm of Cu in a metal vacuum-evaporation apparatus.

Alkanethiolation of the prism was undertaken as described above. ATR-FTIR was undertaken while the front of the prism was exposed to a solution of 0.1 M $CsHCO_3$ under CO_2.

Data Availability Statement

Raw data used in preparation of this manuscript is available to download at (TO BE FILLED AT PROOF STAGE).

References

1. IPCC, 2013. *Climate Change 2013: The Physical Science Basis. Contribution of Working Group I to the Fifth Assessment Report of the Intergovernmental Panel on Climate Change*. (2013).
2. Raciti, D. & Wang, C. Recent Advances in CO2 Reduction Electrocatalysis on Copper. *ACS Energy Lett.* **3,** 1545–1556 (2018).
3. Qiao, J., Liu, Y., Hong, F. & Zhang, J. A review of catalysts for the electroreduction of carbon dioxide to produce low-carbon fuels. *Chem. Soc. Rev.* **43,** 631–675 (2014).
4. Sander, R. Compilation of Henry's law constants, version 3.99. *Atmos. Chem. Phys. Discuss.* **14,** 29615–30521 (2014).
5. Hori, Y., Kikuchi, K. & Suzuki, S. Production of CO and CH4 in electrochemical reduction of CO2 at metal electrodes in aqueous hydrogencarbonate solution. *Chem. Lett.* **14,** 1695–1698 (1985).
6. Seymour, R. S. & Hetz, S. K. The diving bell and the spider: the physical gill of Argyroneta aquatica. *J. Exp. Biol.* **214,** 2175–2181 (2011).
7. Wang, J., Zhang, F., Kang, X. & Chen, S. Organic functionalization of metal catalysts: Enhanced

activity towards electroreduction of carbon dioxide. *Curr. Opin. Electrochem.* **13,** 40–46 (2019).

8. Zhou, Y. *et al.* Dopant-induced electron localization drives CO2 reduction to C2 hydrocarbons. *Nat. Chem.* **10,** 974–980 (2018).

9. Varela, A. S., Kroschel, M., Reier, T. & Strasser, P. Controlling the selectivity of CO2 electroreduction on copper: The effect of the electrolyte concentration and the importance of the local pH. *Catal. Today* **260,** 8–13 (2016).

10. Piontek, S. *et al.* Bio-inspired design: bulk iron–nickel sulfide allows for efficient solvent-dependent CO2 reduction. *Chem. Sci.* **10,** 1075–1081 (2019).

11. Li, Y. *et al.* Structure-Sensitive CO2 Electroreduction to Hydrocarbons on Ultrathin 5-fold Twinned Copper Nanowires. *Nano Lett.* **17,** 1312–1317 (2017).

12. De Luna, P. *et al.* Catalyst electro-redeposition controls morphology and oxidation state for selective carbon dioxide reduction. *Nat. Catal.* **1,** 103–110 (2018).

13. Tang, W. *et al.* The importance of surface morphology in controlling the selectivity of polycrystalline copper for CO2 electroreduction. *Phys. Chem. Chem. Phys.* **14,** 76–81 (2012).

14. Jeon, H. S., Kunze, S., Scholten, F. & Roldan Cuenya, B. Prism-Shaped Cu Nanocatalysts for Electrochemical CO2 Reduction to Ethylene. *ACS Catal.* **8,** 531–535 (2018).

15. Reller, C. *et al.* Electrocatalysis: Selective Electroreduction of CO2 toward Ethylene on Nano Dendritic Copper Catalysts at High Current Density. *Adv. Energy Mater.* **7,** (2017).

16. Dutta, A., Rahaman, M., Luedi, N. C., Mohos, M. & Broekmann, P. Morphology Matters: Tuning the Product Distribution of CO2 Electroreduction on Oxide-Derived Cu Foam Catalysts. *ACS Catal.* **6,** 3804–3814 (2016).

17. Huo, Y., Peng, X., Liu, X., Li, H. & Luo, J. High Selectivity Toward C2H4 Production over Cu

Particles Supported by Butterfly-Wing-Derived Carbon Frameworks. *ACS Appl. Mater. Interfaces* **10,** 12618–12625 (2018).

18. Hoang, T. T. H. *et al.* Nanoporous Copper–Silver Alloys by Additive-Controlled Electrodeposition for the Selective Electroreduction of CO2 to Ethylene and Ethanol. *J. Am. Chem. Soc.* **140,** 5791–5797 (2018).

19. Higgins, D., Hahn, C., Xiang, C., Jaramillo, T. F. & Weber, A. Z. Gas-Diffusion Electrodes for Carbon Dioxide Reduction: A New Paradigm. *ACS Energy Lett.* **4,** 317–324 (2019).

20. Dinh, C.-T. *et al.* CO2 electroreduction to ethylene via hydroxide-mediated copper catalysis at an abrupt interface. *Science* **360,** 783–787 (2018).

21. Huan, T. N. *et al.* Low-cost high-efficiency system for solar-driven conversion of CO2 to hydrocarbons. *Proc. Natl. Acad. Sci. U.S.A* **116,** 9735–9740 (2019).

22. Li, C. W. & Kanan, M. W. CO2 Reduction at Low Overpotential on Cu Electrodes Resulting from the Reduction of Thick Cu2O Films. *J. Am. Chem. Soc.* **134,** 7231–7234 (2012).

23. Mistry, H. *et al.* Highly selective plasma-activated copper catalysts for carbon dioxide reduction to ethylene. *Nat. Commun.* **7,** 12123 (2016).

24. Checco, A., Hofmann, T., DiMasi, E., Black, C. T. & Ocko, B. M. Morphology of Air Nanobubbles Trapped at Hydrophobic Nanopatterned Surfaces. *Nano Lett.* **10,** 1354–1358 (2010).

25. Melnichenko, Y. B. *et al.* Cavitation on Deterministically Nanostructured Surfaces in Contact with an Aqueous Phase: A Small-Angle Neutron Scattering Study. *Langmuir* **30,** 9985–9990 (2014).

26. Zheng, D. *et al.* Salvinia-Effect-Inspired “Sticky” Superhydrophobic Surfaces by Meniscus-Confined Electrodeposition. *Langmuir* **33,** 13640–13648 (2017).

27. Kopljar, D., Inan, A., Vindayer, P., Wagner, N. & Klemm, E. Electrochemical reduction of CO2 to formate at high current density using gas diffusion electrodes. *J. Appl. Electrochem.* **44,** 1107–1116 (2014).

28. Neumann, D. & Woermann, D. Stability of the volume of air trapped on the abdomen of the water spider Argyroneta aquatica. *Springerplus* **2,** 694 (2013).

29. Hokmabad, B. V. & Ghaemi, S. Effect of Flow and Particle-Plastron Collision on the Longevity of Superhydrophobicity. *Sci. Rep.* **7,** 41448 (2017).

30. Huan, T. N. *et al.* Porous dendritic copper: an electrocatalyst for highly selective CO2 reduction to formate in water/ionic liquid electrolyte. *Chem. Sci.* **8,** 742–747 (2017).

31. Huan, T. N. *et al.* A Dendritic Nanostructured Copper Oxide Electrocatalyst for the Oxygen Evolution Reaction. *Angew. Chemie Int. Ed.* **56,** 4792–4796 (2017).

32. Wang, Y., Im, J., Soares, J. W., Steeves, D. M. & Whitten, J. E. Thiol Adsorption on and Reduction of Copper Oxide Particles and Surfaces. *Langmuir* **32,** 3848–3857 (2016).

33. Dilimon, V. S., Denayer, J., Delhalle, J. & Mekhalif, Z. Electrochemical and Spectroscopic Study of the Self-Assembling Mechanism of Normal and Chelating Alkanethiols on Copper. *Langmuir* **28,** 6857–6865 (2012).

34. Aytug, J. T. S. and S. R. H. and T. Superhydrophobic materials and coatings: a review. *Reports Prog. Phys.* **78,** 86501 (2015).

35. Schoenfisch, M. H. & Pemberton, J. E. Air Stability of Alkanethiol Self-Assembled Monolayers on Silver and Gold Surfaces. *J. Am. Chem. Soc.* **120,** 4502–4513 (1998).

36. Singh, M. R., Kwon, Y., Lum, Y., Ager, J. W. & Bell, A. T. Hydrolysis of Electrolyte Cations Enhances the Electrochemical Reduction of CO2 over Ag and Cu. *J. Am. Chem. Soc.* **138,** 13006–13012 (2016).

37. Kortlever, R., Shen, J., Schouten, K. J. P., Calle-Vallejo, F. & Koper, M. T. M. Catalysts and Reaction Pathways for the Electrochemical Reduction of Carbon Dioxide. *J. Phys. Chem. Lett.* **6,** 4073–4082 (2015).

38. Liu, X. *et al.* pH effects on the electrochemical reduction of CO2 towards C2 products on stepped copper. *Nat. Commun.* **10,** 32 (2019).

39. Rahaman, M., Dutta, A., Zanetti, A. & Broekmann, P. Electrochemical Reduction of CO2 into Multicarbon Alcohols on Activated Cu Mesh Catalysts: An Identical Location (IL) Study. *ACS Catal.* **7,** 7946–7956 (2017).

40. Chen, C. S., Wan, J. H. & Yeo, B. S. Electrochemical Reduction of Carbon Dioxide to Ethane Using Nanostructured Cu2O-Derived Copper Catalyst and Palladium(II) Chloride. *J. Phys. Chem. C* **119,** 26875–26882 (2015).

41. Zahiri, B., Sow, P. K., Kung, C. H. & Mérida, W. Active Control over the Wettability from Superhydrophobic to Superhydrophilic by Electrochemically Altering the Oxidation State in a Low Voltage Range. *Adv. Mater. Interfaces* **4,** 1700121 (2017).

42. Eilert, A. *et al.* Subsurface Oxygen in Oxide-Derived Copper Electrocatalysts for Carbon Dioxide Reduction. *J. Phys. Chem. Lett.* **8,** 285–290 (2017).

43. Mo, H. & Raftery, D. Pre-SAT180, a simple and effective method for residual water suppression. *J. Magn. Reson.* **190,** 1–6 (2008).

Supplementary Information

Supplementary Figures 1-21, Supplementary Tables 1-6 and Supplementary Video 1 are provided as Supplementary Materials.

Acknowledgements

V.M. acknowledges financial support from CNRS-Cellule Energie and Fondation of Collège de France for the acquisition of the GC equipment. D.W. was supported by an Idex PSL grant (ANR-10-IDEX-001-02 PSL★), the Fondation of Collège de France and the Marie Curie PRESTIGE Fellowship programme. S.L. was funded by the Corps des Ponts, des Eaux et des Forêts. XRD measurements was carried out by Dr Gwenaelle Rousse at the Collège de France. SEM images were collected by David Montero at the Institut des Matériaux de Paris. BET measurements were carried by Dr Juliette Blanchard at the Laboratoire de Réactivité de Surface at the Université de Pierre et Marie Curie.

Author contributions

D.W., M.F. and V.M. conceived the research. D.W. and S.L. performed electrocatalysis and characterization. N.M. carried out TEM measurements. F.O., S.L. and D.W. carried out IR experiments. XPS was carried out by D.M. and P.M. All authors analyzed the data. D.W. wrote the manuscript. S.L., M.F. and V.M. added to the discussion and contributed to the preparation of the manuscript. M.F. and V.M. supervised the work.

Competing interests: Authors declare no competing interests.

Author Information

*marc.fontecave@college-de-france.fr (M.F.)

*mougel@inorg.chem.ethz.ch (V.M.)

Current address of Victor Mougel: Department of Chemistry and Applied Biosciences, Laboratory of Inorganic Chemistry, Swiss Federal Institute of Technology Zürich, Valdimir-Prelog-Weg 1, 8093 Zürich, Switzerland

END OF MANUSCRIPT